Augmented Forced Convection Heat Transfer in Separated Flow Around a Blunt Flat Plate

K. Hourigan
L. W. Welch
M. C. Thompson
P. I. Cooper
M. C. Welsh
Commonwealth Scientific and Industrial Research Organisation, Division of Building, Construction and Engineering, Highett, Victoria, Australia

■Results of numerical and experimental investigations of large-scale structures, both vortical and thermal, in the separating and reattaching flow on a heated rectangular plate are presented. A two-dimensional acoustic field is applied to lock the rate of vortex shedding from the leading-edge separation bubble and set the mean reattachment length. From autocorrelations and spectral analyses of the forced flow, it is found that large-scale vortex structures form in the separating shear layer at the acoustic forcing frequency and shed into the turbulent boundary layer. Downstream of reattachment, autocorrelations of the velocity fluctuations at a point near the plate show the dominant frequency of the velocity fluctuations to be half the applied acoustic frequency. The level of the applied acoustic field is set to optimize this correlation and to give a frequency comparable to the dominant frequency of vortex shedding in the natural (unforced) shedding case. A qualitative understanding of the instantaneous flow structures and the thermal structures forming on a heated plate is given by visualization using hydrogen bubbles in a water tunnel and Schlieren photography, respectively. A two-dimensional numerical model is used to predict the instantaneous flow structures and thermal field; good qualitative agreement is found between the predictions and the observations. Interpretation is made of the increased heat transfer rate on the plate surface as a result of the action of the large-scale vortex structures.

Keywords: *augmentation, flow convection, flow separation, flow visualization*

INTRODUCTION

In recent years, great interest has been shown in the study of the flows around thick plates with sharp leading-edge corners [1-12]. The plates used in these studies have flow separating from near the leading edge and reattaching further downstream, thus forming a separation bubble. This separation leads to an increase of about 30-50% in the time-mean rate of heat transfer in comparison with that measured for an attached turbulent boundary layer on a heated flat plate [1]. The potential of using rectangular tubes in compact heat exchangers to increase the convective heat transfer coefficient has been demonstrated [13, 14]. To obtain the maximum benefit from tube shapes that induce separated flows near their leading edge, it is necessary to understand the influence that vortex structures resulting from flow separation have on the heat transfer process. Patera and Mikic [15] have used this approach in investigating heat transfer in resonant flow around a cylinder.

At the point of reattachment downstream of the leading edge of a blunt flat plate, a linear log-log relationship exists between the time-mean local Nusselt and Reynolds numbers, where both are based on the reattachment length. Also the rate of convective heat transfer increases as the reattachment length decreases, independent of whether this length is reduced by changing the leading-edge geometry from square to a sharp wedge shape [16] or applying a controlling sound field [17]. Other studies for different geometries have shown that reattachment lengths can also be reduced as a result of acoustic forcing (eg, flow over the blunt leading edge of a circular cylinder [18]).

The studies of Parker and Welsh [7], Cherry et al [11], and Kiya and Sasaki [5] have examined the *instantaneous* flows associated with the reattaching process for plates with square leading edges. These studies show that reattachment is associated with large-scale vortex structures being shed into the boundary layer. Separating and reattaching shear layers are characterized by the successive vortex mergings, leading eventually to the shedding of these large-scale vortex structures [11]. There are two fundamentally different instabilities involved: first, there is the Kelvin-Helmholtz instability of the free shear layer; second, there is the "shedding" type of instability of the entire bubble, which results in the large-scale structures being released into the boundary layer [19].

In an unforced flow around a rectangular plate, the large-scale structures that form in the separating shear layer are released from the separation bubble over a broad range of frequencies [5, 19]. In the present study, sound is applied at an amplitude and frequency that results in the shedding of large-scale structures from the bubble at close to the domi-

Address correspondence to Mrs. C. Bowditch, CSIRO Division of Building, Construction and Engineering, P. O. Box 56, Highett, Victoria 3190, Australia.

Experimental Thermal and Fluid Science 1991; 4:182-191

nant frequency found for natural shedding. In effect, the flow becomes a highly periodic version of the unforced case. The potential for phase-averaging techniques to investigate the instantaneous velocity and thermal fields is therefore maximized. Other studies have used sound to stimulate the flow (eg, [20]), but usually no attempt has been made to optimize the correlation between the sound and vortex shedding.

Kiya et al [3] and Nagano et al [21] studied the flow around plates with square leading edges using numerical methods (discrete-vortex method). In these models, elemental vortices that model the separating shear layer are released from near the leading-edge corners of the plate. Thompson et al [22] combined a discrete-vortex flow solution with a finite-difference solution of the advective heat equation to study the unsteady forced convection around a semiinfinite flat plate with a square leading edge, and showed that the profile of the local Nusselt number along the plate surface could be successfully predicted.

The present paper describes both numerical and experimental studies that examine the instantaneous forced convection flow over a heated plate with a square leading edge when an applied sound field is used to "control" the flow. The aims of the study are to investigate the vortex shedding from the separation bubble through the application of sound at a sound pressure level and frequency that optimizes the correlation of the vortex shedding and to determine the relationship between the large-scale vortex structures and the thermal structures through the combined results of hot-wire anemometry, flow visualization in a water tunnel, Schlieren photography, and numerical techniques, each of which provides a different perspective on the flow. Since it is known that the large-scale flow structures are similar over a wide Reynolds number range [4], it is possible to draw general conclusions on the role of the large-scale structures in the convective heat transfer process from the limited number of tests described in this paper.

TEST APPARATUS AND PROCEDURES

Experiments described in this paper were carried out in both air and water tunnels.

Air Tunnel and Instrumentation

For the experiments in air, the major components of the test apparatus were two small blowdown open-jet wind tunnels (Fig. 1), which are described by Parker and Welsh [7] and Welsh et al [8]. In both tunnels, air was supplied by a centrifugal fan powered by a variable-speed motor. Flow from the fan was directed through a diffuser to a settling chamber containing screens and a honeycomb designed in accordance with the recommendations of Loehrke and Nagib [23, 24] for minimizing turbulence levels. The air then passed through an 8:1 contraction to form an open jet with an outlet that was 244 mm square.

The operating range of the tunnel with the smaller fan fitted was 0–15 m/s; for the tunnel with the larger fan fitted, it was 4–40 m/s. The mean velocity profile in the core of the jet in the working section of each tunnel was uniform within ±0.5%, while the longitudinal turbulence level was typically 0.3% when bandpass-filtered between 0.1 Hz and 2 kHz. The spectrum of the fluctuating longitudinal velocity had no sharp peaks and decreased continuously in amplitude by 55 dB from 0.1 Hz to 2 kHz.

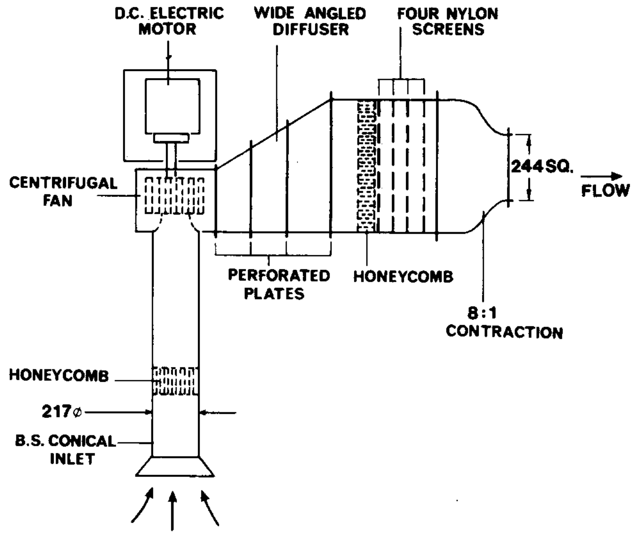

Figure 1. Schematic of open-jet wind tunnel.

The hot-wire studies were undertaken in the tunnel with the smaller fan installed. The plate used for these studies was machined from a block of aluminum so that the corners at the leading and trailing edges were sharp and at 90°. The plate was 13 mm thick and 130 mm long, with a span across the flow of 135 mm and therefore fitted entirely into the core of the flow in the working section (Fig. 2). A sound field was imposed on the flow by locating one speaker above the plate and another below the plate (Fig. 2). The speakers were positioned just outside the jet, 350 mm apart, and were connected in antiphase to generate an acoustic standing wave across the flow. The acoustic particle velocities, which oscillate in phase around the leading and trailing edges of the plate, are superimposed on the mean flow at the applied acoustic frequency. The acoustic particle velocity amplitude was a maximum at the leading and trailing edges and was zero on the plate surface midway along the chord. Near the plate this acoustic field is equivalent to a resonant Parker β-mode as described by Parker and Welsh [7]. The harmonics of the sound generated by the speakers were at least 30 dB below the fundamental. Glass end plates fitted to the plate ensured that the sound field around the plate was two-dimensional.

The largest surfaces of the plate were aligned parallel to the upstream flow direction by balancing the mean total

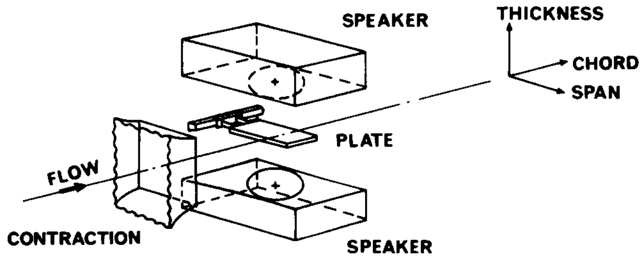

Figure 2. Schematic of the working section of the open-jet wind tunnel.

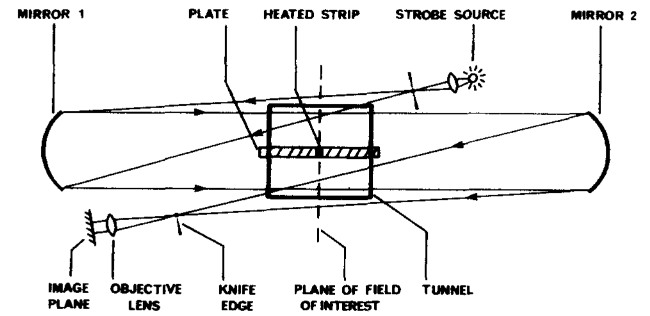

Figure 3. Schematic of test apparatus for Schlieren photography. Incident airflow is into page.

pressure readings on the top and bottom surfaces midway between the leading and trailing edges. The maximum difference was $0.02 \times \frac{1}{2}\rho_f U^2$. Instantaneous flow velocities in the mean flow direction were measured in a plane 1.39 plate thicknesses above the plate with a constant-temperature hot-wire probe with the sensor aligned parallel to the leading edge of the plate and at right angles to the mean flow direction. The fluctuating flow velocity signal was digitized at 9000 Hz and bandpassed between 10 and 3000 Hz before processing on a PDP-11/44 minicomputer; at the same time, the mean flow parameters were recorded and the mean flow velocity calculated.

The Schlieren photography was undertaken in the tunnel with the larger fan fitted. A simple Schlieren optical system was installed around the open-jet working section to observe the instantaneous density gradient field around the plate (see Fig. 3). The plate used in these experiments had the same geometry as the plate constructed from aluminum but was constructed from wood. In addition, end plates were not used because of their interference with the optics of the Schlieren system. Because a Schlieren system detects density gradients (transverse to the knife edge) existing at all points along a collimated beam, it was necessary to achieve a narrow spanwise thermal field by placing a 2 mm wide heater strip of 76 μm thick stainless steel around the plate at the midspan position. Electrical connections to a stabilized ac power supply were made on the trailing edge. The heater strip approximated a constant heat flux surface with negligible radiant heat transfer.

Water Tunnel and Instrumentation

The test rig (a return circuit water tunnel), shown in Fig. 4, was also designed using well-accepted principles for minimizing the free-stream turbulence level in the working sections of air tunnels [23, 24]. Water was pumped into a settling chamber containing filter material and a honeycomb and then passed through a two-dimensional 4:1 contraction before entering the working section, which was 770 mm long and was constructed from 25 mm thick acrylic supported in aluminum flanges.

The maximum mean flow velocity in the working section was 400 mm/s, and the mean velocity profile between the boundary layers was uniform within 0.5%. The longitudinal turbulence level was typically 0.1% when bandpass-filtered between 0.08 and 20 Hz. The spectra of the fluctuating longitudinal velocity had no sharp peaks and decreased continuously in amplitude by 20 dB/Hz from 0.08 Hz.

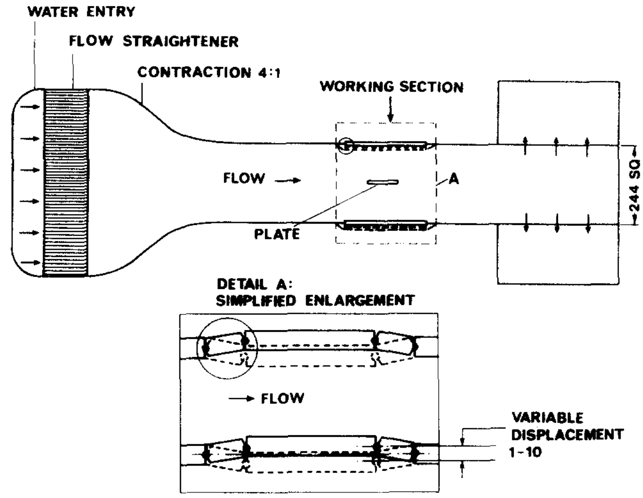

Figure 4. Schematic of the return circuit water tunnel showing the oscillating side walls of the working section.

Two panels in the side walls of the working section were rigidly connected to each other and were sealed to the remainder of the working section by a thin flexible membrane. This construction permitted the side-wall panels to be oscillated transverse to the mean upstream flow direction, thus superimposing a transverse flow velocity perturbation onto the flow near the plate. The velocity perturbation near the plate produced by the speakers in the air tunnel and the oscillating side walls in the water tunnel are similar. The oscillation of the sides walls could be varied from 0 to ± 5 mm at frequencies between 0 and 6 Hz. The oscillation of the side walls was essentially sinusoidal, with the velocity amplitudes of the higher harmonics at least 20 dB less than the fundamental, except for the third harmonic, which was 10 dB less. When a plate was located in the working section between the oscillating walls, a transverse flow velocity perturbation up to 150 mm/s could be imposed on the flow surrounding the body.

The plate used in the water tunnel had the same geometry as the aluminum one described above but was constructed from acrylic to prevent corrosion and for ease of flow visualization, which was achieved using the hydrogen bubble technique [25, 26]. A nichrome wire was located on the leading surface of the plate at a point midway between the corner and the plane of symmetry through the plate. Hydrogen bubbles, which were generated by passing a 0.15 A direct current through the nichrome wire, were shed into the shear layer separating from the leading-edge corner. White light was used to illuminate the bubbles and show the details of the instantaneous flows around the plate. Video recordings and photographs of the flow around the plates were taken from above the tunnel or through the oscillating side walls (Fig. 4).

Experimental Procedures

For the experiments described in this paper that were performed in air, the sound was applied at a frequency of 135 Hz with a sound pressure level of 115 dB (reference 20 μPa) at the middle of the plate. For the water tunnel experiments, transverse wall displacements of 0.025 mm were imposed at 5.2 Hz on the flow, which had a mean velocity of 93.6 mm/s.

The Reynolds number was 7800 for the hot-wire data, 6140 for the Schlieren photography, and 1200 for the water tunnel, where the Reynolds number was based on plate thickness for each case. Although these experiments are for specific Reynolds numbers covering a limited range, Kiya and Sasaki [4] showed that the large-scale flow structures in a separating and reattaching flow are similar over a wide Reynolds number range (from 640 to 2.6×10^4). This permits generalized conclusions to be drawn from the tests described in this paper. The Strouhal number, based on the controlling perturbation frequency and plate thickness, was approximately 0.2 in all cases with a maximum controlling velocity perturbation at the center of the leading edge of the plate of 0.05, normalized to the free-stream velocity.

EXPERIMENTAL ERRORS

The conclusions put forward in the paper are not critically dependent on the measurement accuracy of the results. However, appropriate procedures were adopted to ensure both a high level of measurement accuracy and repeatability.

Positional Accuracy

The initial positions of the hot-wire probes were determined with the aid of a helium-neon laser. The relative positional adjustments were made by using precision machine slides. Positional inaccuracy was less than 0.2 mm. All other data were collected by using a laboratory peripheral accelerator (LPA) on a Digital Equipment Corp. PDP-11/44 minicomputer. Calibrations were made with transducer and intermediate components up to and including the analog-to-digital converter in the LPA.

Accuracy after Calibration

- *Fluctuating velocities*. Thermal Systems Inc. miniature constant-temperature hot-wire probes; velocity measurement tolerance <0.1 m/s, frequency response to 15 kHz.
- *Ambient temperature*. Copper-constantan thermocouple with high-gain amplifier, temperature accuracy tolerance <0.5 K.
- *Atmospheric pressure*. Druck pressure transducer, <0.1 kPa.
- *Sound pressure*. WAVETEX Model 145 signal generator, Hewlett-Packard frequency counter (<1 Hz), and Bruel and Kjaer 12.7 mm condenser microphone (<0.5 dB).
- *Mean flow velocity*. British Standard conical inlet, pressure differential Setra transducer ($<2\%$).
- *Density gradients*. The Schlieren system was used for qualitative flow visualization; no formal calibration of the equipment was made to relate density gradients in the image to temperature gradients. However, relating the observations to the numerical simulations, it could be estimated that with the heated strip and free stream at approximately 70°C and 20°C, respectively, there would be a drop of 45 K in the first 1 mm near the heated plate surface. Because the large-scale structures were of prime interest, the sensitivity of the Schlieren system was adjusted to reveal gradients of approximately 0.5 K/mm.

DESCRIPTION OF THE NUMERICAL MODEL

This study is concerned primarily with the time-dependent structures found in the flow. Ideally, the time-dependent Navier-Stokes and advective heat equations must be solved. However, for high Reynolds number flow, this is computationally very expensive; extremely fine grid resolution is required, especially around the sharp leading-edge corner. It was decided that for the present study, a hybrid scheme using a vortex model that had been successfully tested [22] combined with a high-order finite-difference approximation to the advective heat would provide at least a qualitative picture of the velocity and thermal fields and assist in the interpretation of the experimental results.

The discrete-vortex method has been used successfully by Kiya et al [3] to model the large-scale (two-dimensional) structures shed from a turbulent separation bubble. The method involves releasing elemental vortices at discrete time intervals from the leading-edge corners of the plate. Large-scale vortex structures then manifest as clouds of these elemental vortices. However, in order to match experimentally observed features such as the mean separation length, it was found necessary in the study of Kiya et al [3] to reduce the strengths of elemental vortices in an ad hoc manner. A similar discrete-vortex method has been used recently by Basuki and Graham [27] to model the flow around an inclined airfoil. In the study by Thompson et al [22], a self-consistent scheme was employed to account for the cross-annihilation of primary vorticity by vorticity generated downstream of the leading edge; this represented an improvement on the ad hoc vorticity decay used in other vortex models. The large-scale structures that dominate the energy transfer were found to be modeled satisfactorily. Vortex models, based on the schemes used by Spalart et al [28] and Speziale et al [29], where elemental vortices are released over the entire body, are satisfactory for modeling trailing edge separation or where strong forcing is applied [30]. However, this method was found to produce unrealistically short separation bubbles for the present geometry, probably owing to high levels of numerical noise in the separating shear layer induced by the recirculating elemental vortices formed downstream of the leading-edge corner.

The plate is assumed to be semiinfinite with parallel sides and a square leading edge aligned normal to the two-dimensional incompressible flow, which has uniform velocity and uniform temperature at upstream infinity.

Discrete Vortex Model

The discrete-vortex model used here has been described previously in Thompson et al [22]. This method models the shear layer separating from the leading-edge corner of the plate by introducing vortex blobs, with Rankine profile, into the flow at sufficiently high frequency to simulate the smooth shear layer observed experimentally. The strength and position of the elemental vortices are determined through satisfying the Kutta condition. Furthermore, the present scheme contains a refinement that accounted for the annihilation of the primary vorticity shed at the leading edge by vorticity of

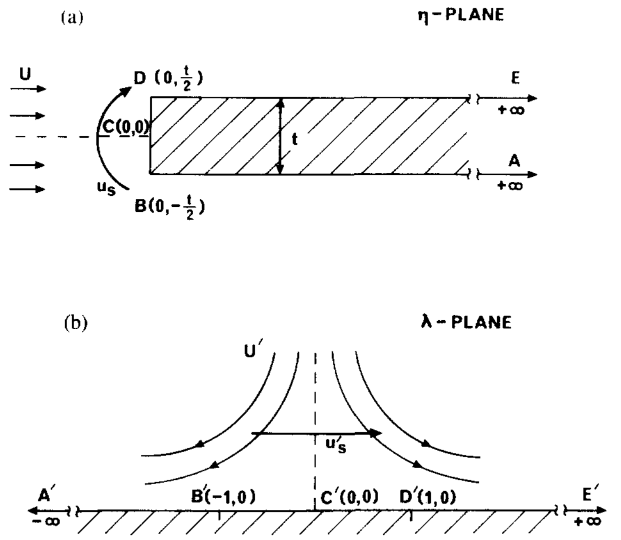

Figure 5. Conformal mapping for the vortex cloud model.

opposite circulation that enters the flow downstream of separation, as detailed in [22].

The local fluid velocity is determined kinematically from the vorticity field and the irrotational field. The potential fields are obtained by using a Schwarz-Christoffel transformation to project the exterior region of the plate (η plane) into the upper half-plane (λ plane) with the boundary of the plate along the real axis (see Fig. 5). The inviscid motion of the elemental vortices is then determined from the velocity potential in the transformed plane. The conformal transformation used is the inverse of

$$\eta = \left\{\lambda(\lambda^2 - 1)^{1/2} - \log\left[\lambda - (\lambda^2 - 1)^{1/2}\right]\right\}\frac{t}{\pi} + i\frac{t}{2} \quad (1)$$

The points $\eta = -it/2$ and $\eta = +it/2$, which represent the lower and upper leading edge corners, respectively, are mapped into $\lambda = -1$ and $\lambda = +1$.

The complex potential ϕ at position λ is then given by

$$\phi(\lambda, \tau) = \left[U\lambda^2 + 2V'\lambda\sin(2\pi f\tau)\right]\frac{t}{\pi} + \sum_j iG_j\left[\log\left(\frac{\lambda - \lambda_j}{\lambda - \lambda_j^*}\right)\right] \quad (2)$$

where the potential due to image vortices (third term on the right) has been introduced to satisfy the zero-mass flux condition at the plate surface. Here, the asterisk denotes a complex conjugate. The second term on the right is the local potential flow approximation to the long-wavelength transverse resonant acoustic field, where V' is the magnitude of the acoustic particle velocity at the center of the leading edge of the plate and f is the frequency of the acoustic field.

At positions other than vortex centers, the flow velocity is given by $d\phi/d\eta$. The well-known Routh correction is applied to obtain the limiting velocity at the center of the kth vortex, that is, $\lim_{\eta \to \eta_k}(d/d\eta)[\phi - iG_k \log(\eta - \eta_k)]$. The position of each vortex is then advanced using a second-order Euler scheme. The time step used is $0.05t/U$, and an elemental vortex is introduced at every fourth time step. This period is sufficiently small relative to the sound period [$O(10^2)$ time steps] to enable a good approximation to a continuous shear layer to be obtained.

The circulation of each elemental vortex introduced at the leading edge is determined in a manner similar to that of Nagano et al [21]. That is, the rate of shedding of vorticity is determined from $dG/d\tau = 1/2\,V_s^2$, where V_s is the velocity at the outer edge of the boundary layer separating from the leading edge of the plate. The thickness of this boundary layer is taken to be $0.02t$, consistent with the value predicted by stagnation boundary layer theory for flows of Reynolds number of the order 10^3 and length scale of the order t [31].

Finite-Difference Solution of the Heat Equation

The advective heat equation for the fluid is given by

$$\frac{\partial T}{\partial \tau} + \mathbf{u} \cdot \nabla T = \frac{\kappa}{\rho_f C_p} \nabla^2 T \quad (3)$$

This is solved using a flux-limiting scheme [32]. This method uses a combination of higher- and lower-order finite-difference approximations to model convection-dominated flows. On a cell-by-cell basis, the higher-order approximation is used unless it would result in nonphysical fluxes into a cell, in which case the lower-order (but stable) approximation is used instead. This prevents the "wiggly" solutions (such as those resulting from the use of central differences on coarse grids) from developing. The higher-order finite-difference scheme is QUICKEST [33], which employs explicit third-order upstream differencing for the advection terms and an advective approximation to the truncated time difference terms similar to that used for Leith's method [34]. The lower-order scheme is a first-order donor cell method. The difference approximations are calculated on a compressed mesh of size 51×31 (Fig. 6). This mesh consists of two rectangular grid systems in a transformed upper half-plane compressed toward the plate surface and joined near the leading-edge corner. Because the maximum time step for stability is proportional to the smallest cell dimension (due to the Courant-Friedrichs-Lewy condition), the composite mesh has the advantage of a much larger maximum time step. No instabilities were observed to propagate from the interface between the meshes.

The boundary conditions used in the model are constant heat flux at the plate surface, constant ambient temperature at the boundary away from the plate surface, and zero temperature gradients at the two outflow boundaries (one downstream from the leading edge and the other near the opposite leading-edge corner). The application of the zero-gradient boundary condition near the leading-edge corner on the lower

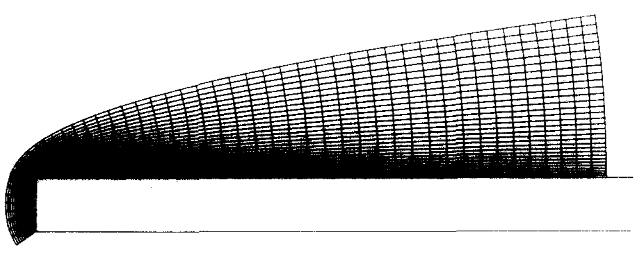

Figure 6. Mesh used for finite-difference solution of advective heat equation.

surface is satisfactory, because the solution is sought only for the top surface of the plate. The grid was extended past the extreme position of the stagnation streamline, ensuring that there was little feedback effect on the thermal field on the top half of the plate.

The vectorized code was run on a Cyber 205 computer.

RESULTS

Experimental Flow Results

Averaged correlations of the fluctuating velocities, in the case of applied sound with St = 0.2, are shown in Fig. 7*a* for two different positions along the plate near the point of the time-mean reattachment. These were obtained from the air tunnel by using a hot-wire positioned 1.39 plate thicknesses above the surface. Between points approximately 2 and 3 plate thicknesses from the leading edge along the plate, the autocorrelation coefficient at the applied sound frequency is found to decrease markedly, leaving an autocorrelation coefficient at half the applied sound frequency. In Fig. 7*b*, the autocorrelation at the trailing edge is seen to consist predominantly of a frequency of value half the applied sound frequency, the applied frequency making little contribution. Also shown in Fig. 7*b* are the autocorrelations at the trailing edge of the fluctuating velocities in the case of no applied sound, showing no significant autocorrelations present, as observed by Cherry et al [11]. The data in this figure were obtained by processing continuous time histories for a duration of 120 acoustic cycles.

Photographs of the flow visualization in the water tunnel using hydrogen bubbles for both unperturbed and perturbed cases are shown in Fig. 8. The application of the transverse perturbation leads to a reduction of the separation bubble length and a strong correlation of the vortex shedding frequency with the applied perturbation frequency.

Experimental Thermal Field Results

Figure 9*a* shows a Schlieren photograph of the flow for an acoustic Strouhal number of approximately 0.2 and Peclet number 6140. To highlight the structures, the picture has been digitally enhanced by filtering the photographic image and also tracing along the line of maximum gradient starting from the leading-edge corner of the plate. The resulting enhancement and bounding contour of the large-scale structures are shown in Fig. 9*b*. The vertical density gradients are shown by the shade of grey. Darker regions indicate that the density gradient is positive in the upward direction, whereas the lighter regions indicate a density gradient in a opposite direction.

Predicted Flow and Thermal Fields

The time-mean local Nusselt numbers along the plate predicted by the model are shown in Fig. 10 for flow with and without acoustic forcing. These were obtained by averaging over a period equivalent to eight acoustic cycles due to computer time limitations. Without sound, the shedding is fairly sporadic, and an accurate Nusselt number prediction really requires a longer averaging period. Therefore it is likely that the local minimum downstream of reattachment is

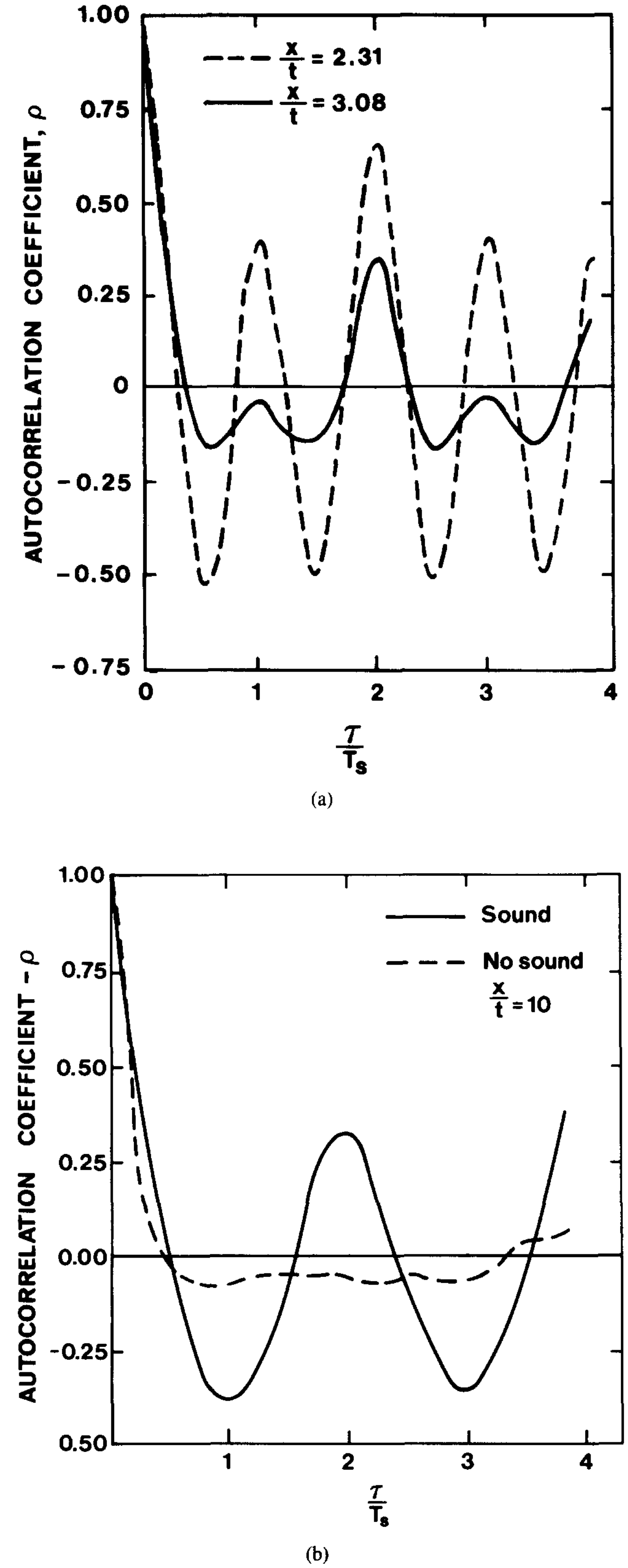

Figure 7. (a) Autocorrelation coefficient of velocity fluctuations 1.39 plate thicknesses above the plate with sound applied, St = 0.2 and U = 9.0 m/s. (b) Autocorrelation coefficient of velocity fluctuations 1.39 plate thicknesses above the trailing edge, St = 0.2 and U = 9.0 m/s.

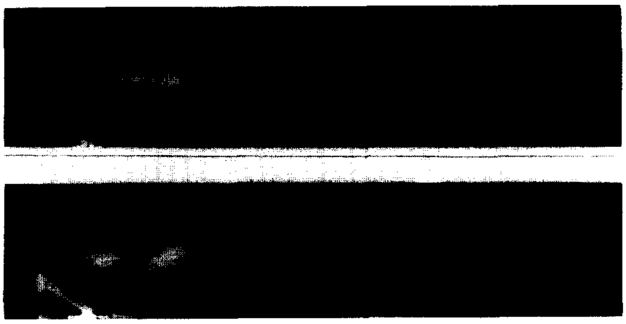

Figure 8. Flow visualization using hydrogen bubbles in the water tunnel showing large-scale structures in the flow around the plate at 96 mm/s for the two cases: (a) no applied perturbation; and (b) an applied perturbation at a forcing St = 0.2 (oscillation frequency 1.5 Hz).

a slight statistical fluctuation due to the short sampling time and has no physical significance.

The discrete-vortex model predicts a flow field that consists of clouds of elemental vortices embedded in an irrotational field. Figure 11*a* shows an instantaneous "snapshot" of the predicted vector velocities of the elemental vortices for the case of acoustic forcing at St = 0.2. For the same instant in time, Fig. 11*b* shows the predicted instantaneous isotherms, and Fig. 11*c* shows the predicted instantaneous local Nusselt number along the plate surface for a Peclet number of 1000.

DISCUSSION

The results of the autocorrelations of the fluctuating velocities shown in Fig. 7*b* for no applied sound show that the vortex shedding frequency extends across a broad band. This result is consistent with the findings of Kiya et al [3] and Cherry et

(a)

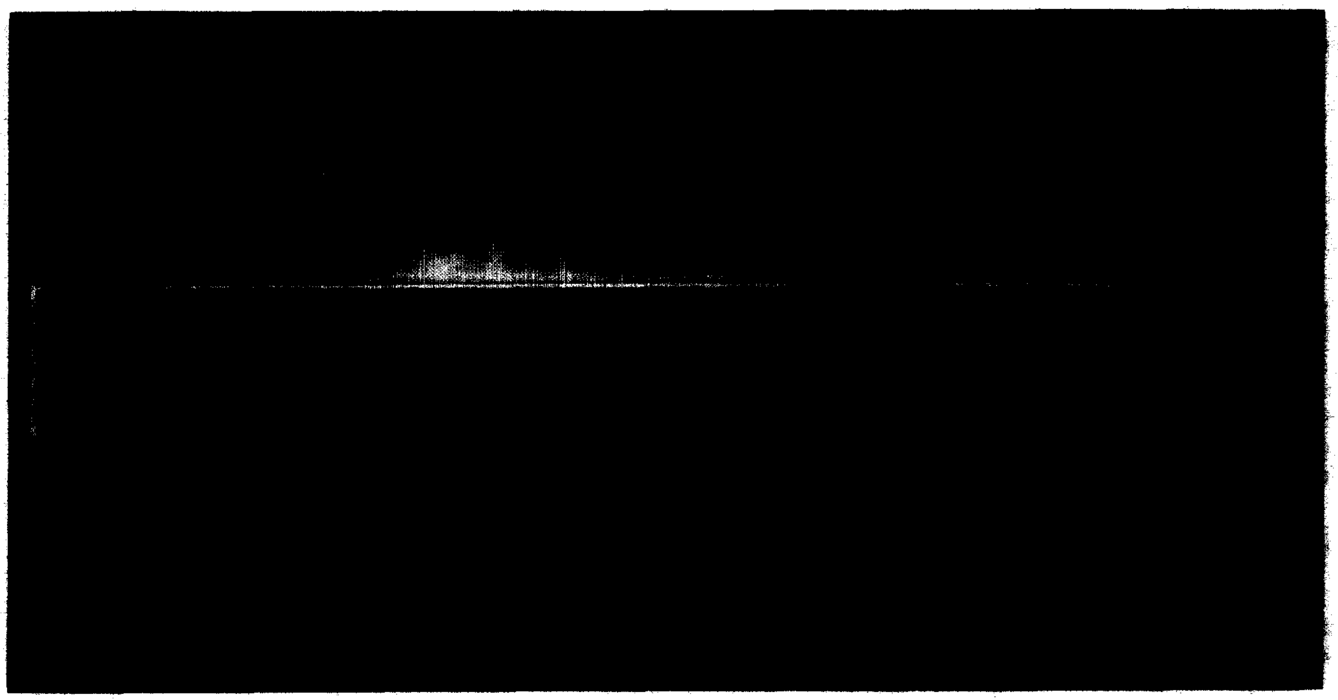

(b)

Figure 9. (a) Schlieren photograph of the flow, from left to right, over the square leading-edge plate for St = 0.2 and Pe = 6140. (b) Digitally enhanced image of (a). Dotted line shows boundary of thermal structures defined by the trace of the maximum local gradient of the image beginning at the leading-edge corner.

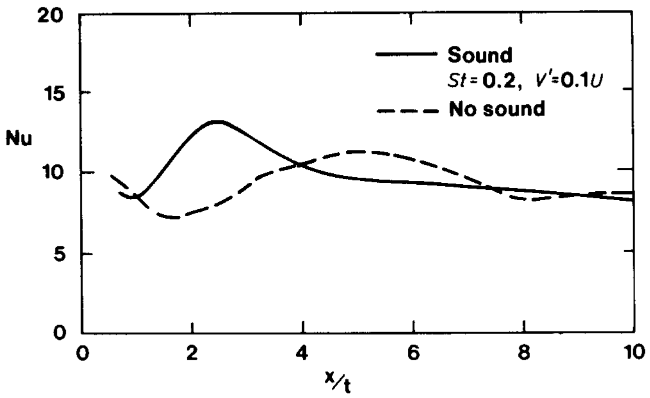

Figure 10. Predicted mean local Nusselt numbers on a plate with a square leading edge for Pe = 1000.

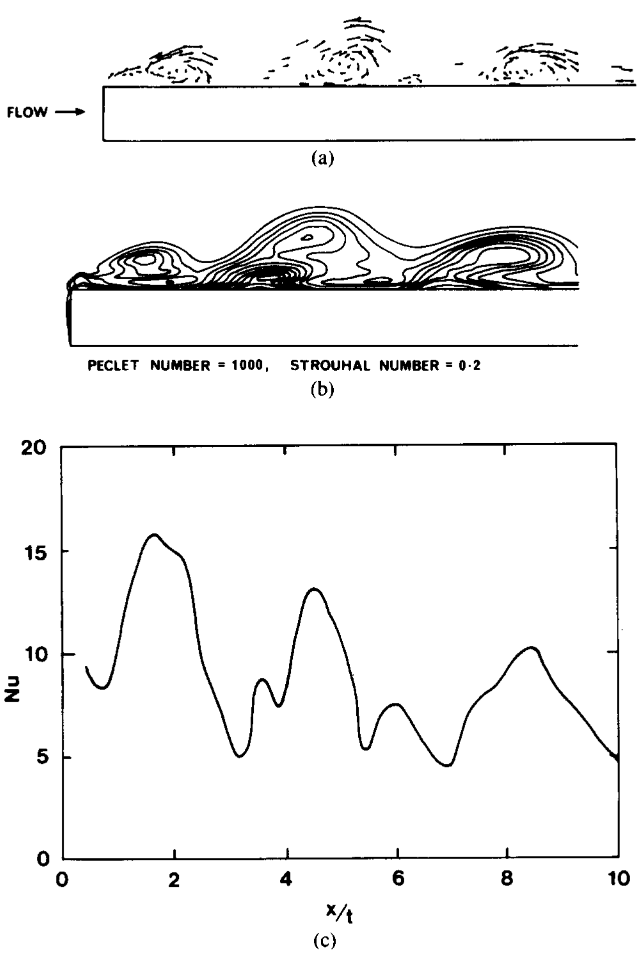

Figure 11. (a) Typical predicted instantaneous "snapshot" of the predicted velocity vectors of the elemental vortices; flow is from left to right, with arrows showing relative magnitude and direction of velocities. (b) Predicted instantaneous isotherms for the flow. (c) Predicted instantaneous Nusselt numbers along the plate surface; St = 0.2, $V' = 0.1U$, and Pe = 1000.

al [11]. In contrast, measurements of the velocity fluctuations in the acoustically forced flow downstream of reattachment at 1.39 plate thicknesses above the plate show a strong autocorrelation downstream of reattachment at half the forcing frequency. This frequency halving is possibly due to three-dimensional effects; current investigations on this aspect of the flow will be described in a future report. A consequence of the lack of coherency in the unforced case is that it restricts the effectiveness of experimental techniques such as phase averaging that could be used to obtain statistics for such flows. This is one reason acoustic flow control is a useful technique; it enables mean flow statistics to be measured from a reasonable number of averages. It is for this reason that the present line of approach to use sound to structure the flow has been adopted. Acoustic forcing can also be used to control the separation bubble length, thereby allowing the effect of this length on the heat transfer to be assessed.

The results from the numerical model shown in Fig. 11 show large-scale vortex patterns consistent with the water tunnel flow visualization in Fig. 8. When the transverse perturbation is applied, the leading-edge separation bubble shortens and periodic vortex shedding results.

Comparing Fig. 10 with the results of Ota and Kon [1] and Copper et al [17], it is found that the model predicts at least the correct qualitative variation of the time-mean Nusselt number along the plate surface. That is, a maximum in the Nusselt number occurs near reattachment with a local minimum in the bubble. The effect of decreasing the reattachment length as a result of applying a transverse sound field is to increase the maximum mean Nusselt number as well as to shift the location at which this maximum is found toward the leading edge. Integration of the Nusselt number along the surface of the plate, which gives a quantity proportional to the total heat transfer rate, shows that the acoustically forced case has an increased overall heat transfer rate similar to that found by Cooper et al [17].

The Schlieren photograph in Fig. 9 shows large-scale thermal structures and thermal gradient patterns similar to those predicted by the model (Fig. 11*b*). A temperature gradient reversal in the separation bubble is indicated by the "winding back" of the numerically predicted temperature contours (Fig. 11*b*) and by the dark regions within the large-scale structures (particularly the leading-edge separation bubble) in the Schlieren photograph and its enhanced image (Figs. 9*a* and 9*b*). At the same instant in the shedding cycle, the thermal structures predicted by the model are associated with a large-scale vortex structure. Similarly, the large-scale structures in the Schlieren photograph and its enhancement (Figs. 9*a* and 9*b*) are closely associated with the large-scale vortex structures in the flow visualization (Fig. 8). It is clear that the large-scale vortex structures play an important role in the transport of energy in the flow and strongly determine the large-scale structures appearing in the thermal field.

Associated with each predicted large-scale vortex structure shown in Fig. 11*a* and its corresponding large-scale thermal structure (Fig. 11*b*) is a local maximum in the instantaneous Nusselt number at the plate surface (Fig. 11*c*). The pattern of the predicted isotherms suggests the strong influence the vortices have on augmenting the heat transfer. The rotational motion induced by a vortex results in heated fluid near the plate surface upstream of the vortex being moved to the outer cooler flow and cooler fluid from the outer flow being transported toward the plate surface downstream of the vortex. The vertical transfer of heat effected by the vortices results in improved heat transfer from the plate surface. In particular, it leads to the local maximum of the Nusselt number at the plate surface under each vortex structure, where the cooled fluid is transported back toward the plate surface. Similarly, near reattachment of the leading-edge separating shear layer, cooler fluid from the outer flow is directed toward the plate surface, contributing to a local maximum in the Nusselt number. Under the leading-edge separation bubble, which contains recirculating flow, the Nusselt number attains a local minimum.

The leading-edge separation bubble, which is a region of relatively poor heat transfer, is reduced in size by the influence of sound. This reduction leads to an increase in the overall heat transfer rate along the plate surface. Of course, the extreme case where the separation bubble is completely eliminated—for example, where the leading edge shape is aerodynamic—results in a laminar boundary layer and a much lower heat transfer coefficient. This study has not attempted to investigate the leading-edge reattachment length that leads to the optimal heat transfer coefficient for the plate. In general, it can be concluded that causing the flow to separate and reattach leads to augmentation of the heat transfer through the action of vortical stirring of the flow, and modification of the flow separation through an external forcing such as sound can optimize the augmentation by reducing the length of the leading-edge separation bubble, which is a region of relatively poor heat transfer.

PRACTICAL USEFULNESS AND SIGNIFICANCE

The results of this study indicate that the increased periodicity when sound is imposed on the flow makes the use of sound an effective method for increasing and controlling the rate of heat transfer while exploring the mechanisms of augmented forced convection. The major flow structures associated with separating and reattaching flows remain when sound is applied. The sound can be used to reduce the separation bubble length and augment the heat transfer. The similarity of the mean heat transfer coefficient and the common presence of large-scale structures in flows resulting from different methods of establishing reattachment length give practical relevance to the present study. This similarity suggests that there is a good possibility that the results with sound will suggest more practicable methods, such as geometry changes, of augmenting heat transfer.

CONCLUSIONS

Various experimental and numerical techniques have been employed to investigate the augmentation of the heat transfer process when the flow is made to separate at the leading edge of a blunt flat plate. Sound has been used to force the flow to become periodic, with regular vortex shedding from the leading-edge separation bubble at a frequency close to the dominant vortex shedding for natural shedding. This enforced periodicity enables direct comparison of the instantaneous flow patterns observed when using hydrogen bubble visualization in a water tunnel with those predicted numerically.

Large-scale thermal structures are found to be associated with the large-scale vortex structures by comparing the water tunnel and predicted results with Schlieren photography performed in a wind tunnel. The large-scale vortex structures shed into the boundary layer of the plate play an important role in the augmentation of the Nusselt number by providing vertical displacement of the warmer fluid near the heated plate surface. Reduction of the leading-edge reattachment length, which has been found to lead to an increase in the mean Nusselt number for a heated plate, can be obtained through the application of sound.

The procedure of controlling the flow with sound is useful in experimental rigs to obtain a periodic flow that allows phase-averaging techniques and direct comparisons with predictions. In practical applications, similar augmentation of the heat transfer process can be obtained by geometrical modifications, such as varying the nose shape of the plate.

We wish to thank Mr. N. B. Hamilton for photographing the flows described in this paper, and Mr. I. G. Pearson for producing the digitally enhanced image.

NOMENCLATURE

C_p heat capacity of fluid at constant pressure, J/K
f acoustic frequency, Hz
G circulation of elemental vortex, m^2/s
i $\equiv \sqrt{-1}$
Nu Nusselt number—ratio of total heat transfer to conductive heat transfer (based on plate thickness and temperature difference between plate and fluid at upstream infinity), dimensionless
p instantaneous acoustic pressure, Pa
P maximum acoustic pressure, Pa
Pe Peclet number ($= C_p \rho_f Ut/\kappa$)—ratio of heat transfer rate due to convection to that due to conduction (based on plate thickness and flow velocity at upstream infinity), dimensionless
R point of flow reattachment, m
Re Reynolds number ($= Ut/\nu$), dimensionless
St Strouhal number ($= ft/U$), dimensionless
t plate thickness, m
T temperature of the flow, K
T_s period of acoustic cycle, s
$\mathbf{u}$ local flow velocity, m/s
u_s acoustic particle velocity, m/s
u'_s acoustic particle velocity in transformed plane, m/s
U mean free-stream velocity at upstream infinity, m/s
U' mean free-stream velocity at upstream infinity in transformed plane, m/s
V' maximum acoustic particle velocity at center of leading edge, m/s
V_s velocity at outer edge of separating shear layer, m/s
x distance from plate leading edge in flow direction, m
y distance from midway between leading edge corners above plate, m
z distance across flow from central point on leading edge surface, m

Greek Symbols

δ thickness of separating shear layer, m
η position in complex physical plane, m
κ thermal conductivity of fluid, m^2/s
λ position in complex transform plane, dimensionless
ν kinematic viscosity of fluid, m^2/s
ρ autocorrelation coefficient of velocity perturbations
ρ_f fluid density, kg/m^3
τ time, s
ϕ complex potential of flow, m^2/s

REFERENCES

1. Ota, T., and Kon, N., Heat Transfer in the Separated and Reattached Flow on a Blunt Flat Plate, *ASME J. Heat Transfer*, **96**, 459-462, 1974.
2. Ota, T., and Itasaka, M., A Separated Flow on a Blunt Flat Plate, *J. Fluids Eng.*, **98**, 79-86, 1976.
3. Kiya, M., Sasaki, K., and Arie, M., Discrete-Vortex Simulation of a Turbulent Separation Bubble, *J. Fluid Mech.*, **120**, 219-244, 1982.
4. Kiya, M., and Sasaki, K., Structure of a Turbulent Separation Bubble, *J. Fluid Mech.*, **137**, 83-113, 1983.
5. Kiya, M., and Sasaki, K., Structure of Large-Scale Vortices and Unsteady Reverse Flow in the Reattaching Zone of a Turbulent Separation Bubble, *J. Fluid Mech.*, **154**, 463-491, 1985.
6. Lane, J. C., and Loehrke, R. I., Leading Edge Separation from a Blunt Plate at Low Reynolds Number, *J. Fluids Eng.*, **102**, 494-496, 1980.
7. Parker, R., and Welsh, M. C., Effects of Sound on Flow Separation from Blunt Flat Plates, *Int. J. Heat Fluid Flow*, **4**, 113-128, 1983.
8. Welsh, M. C., Hourigan, K., Welch, L. W., Downie, R. J., and Thompson, M. C., Acoustic and Experimental Methods: The Influence of Sound on Flow and Heat Transfer, *Exp. Thermal Fluid Sci.*, **3**, 138-152, 1990.
9. McCormick, D. C., Test, F. L., and Lessmann, R. C., The Effect of Free-Stream Turbulence on Heat Transfer from a Rectangular Prism, *J. Heat Transfer*, **106**, 268-275, 1984.
10. McCormick, D. C., Lessmann, R. C., and Test, F. L., Heat Transfer to Separated Flow Regions from a Rectangular Prism in a Cross Stream, *J. Heat Transfer*, **106**, 276-283, 1984.
11. Cherry, N. J., Hiller, R., and Latour, M. E. M. P., Unsteady Measurements in a Separated and Reattaching Flow, *J. Fluid Mech.*, **144**, 13-46, 1984.
12. Stokes, A. N., and Welsh, M. C., Flow-Resonant Sound Interaction in a Duct Containing a Plate. II. Square Leading Edge, *J. Sound Vibration*, **104** (1), 55-73, 1985.
13. Zelenka, R. L., and Loehrke, R. I., Heat Transfer from Interrupted Plates, *ASME J. Heat Transfer*, **105**, 172-177, 1983.
14. Mullisen, R. S., and Loehrke, R. I., Enhanced Heat Transfer in Parallel Plate Arrays, ASME Paper No. 83-HT-43, 1983.
15. Patera, A. T., and Mikic, B. B., Exploiting Hydrodynamic Instabilities. Resonant Heat Transfer Enhancement, *Int. J. Heat Mass Transfer*, **29**, 1127-1138, 1986.
16. Ota, T., and Kon, N., Heat Transfer in the Separated and Reattached Flow over Blunt Flat Plates—Effects of Nose Shape, *Int. J. Heat Mass Transfer*, **22**, 197-206, 1979.
17. Cooper, P. I., Sheridan, J. C., and Flood, G. J., The Effect of Sound on Forced Convection Over a Flat Plate, *Int. J. Heat Fluid Flow*, **7**, 61-68, 1986.
18. Sigurdson, L. W., and Roshko, A., Controlled Unsteady Excitation of Reattaching Flow, AIAA Paper No. 85-0552, 1985.
19. Sigurdson, L. W., The Structure and Control of a Turbulent Reattaching Flow, Ph.D. Thesis, California Institute of Technology, 1986.
20. Bhattacharjee, S., Scheelke, B., and Troutt, T. R., Modification of Vortex Interactions in a Reattaching Separated Flow, *AIAA J.*, **24**, 623-629, 1986.
21. Nagano, S., Naito, M., and Takata, H., A Numerical Analysis of Two-Dimensional Flow Past a Rectangular Prism by a Discrete Vortex Model, *Comput. Fluids*, **10**, 243-259, 1982.
22. Thompson, M. C., Hourigan, K., and Welsh, M. C., Numerical Simulation of the Heat Transfer in the Separated and Reattached Flow on a Blunt Flat Plate, *Int. Commun. Heat Mass Transfer*, **13**, 665-674, 1986.
23. Loehrke, R. I., and Nagib, H. M., Experiments on Management of Freestream Turbulence, AGARD Report, R-598, AD-749-891, 1972.
24. Loehrke, R. I., and Nagib, H. M., Control of Free-Stream Turbulence by Means of Honeycombs: A Balance between Suppression and Generation, *ASME J. Fluids Eng.*, **98**, 342-353, 1976.
25. Clayton, B. R., and Massey, B. S., Flow Visualization in Water: A Review of Techniques, *J. Sci. Instrum.*, **44**, 2-11, 1967.
26. Schraub, F. A., Kline, S. J., Henry, J., Runstadler, P. W., and Littell, A., Use of Hydrogen Bubbles for Quantitative Determination of Time-Dependent Velocity Fields in Low-Speed Water Flows, *ASME J. Basic Eng.*, **87**, 429-444, 1965.
27. Basuki, J., and Graham, J. M. R., Discrete Vortex Computation of Separated Airfoil Flow, *AIAA J.*, **25**, 1409-1410, 1987.
28. Spalart, P. R., Leonard, A., and Baganoff, D., Numerical Simulation of Separated Flows, NASA TM 84328, February 1983.
29. Speziale, C. G., Sisto, F., and Jonnavithula, S., Vortex Simulation of Propagating Stall in a Linear Cascade of Airfoils, *ASME J. Fluids Eng.*, **108**, 304-312, 1986.
30. Thompson, M. C., Hourigan, K., Welsh, M. C., and Soh, W. K., Prediction of Vortex Shedding from Bluff Bodies in the Presence of a Sound Field, *Fluid Dyn. Res.*, **3**, 349-352, 1988.
31. Schlichting, H., *Boundary Layer Theory*, McGraw-Hill, New York, 1979.
32. Zalesak, T., Fully Multidimensional Flux-Corrected Transport Algorithms for Fluids, *J. Comput. Phys.*, **31**, 335-362, 1979.
33. Leonard, B. P., A Stable and Accurate Convective Modelling Procedure Based on Quadratic Upstream Interpolation, *Comput. Methods Appl. Mech. Eng.*, **19**, 55-98, 1979.
34. Leith, C. E., Numerical Simulation of the Earth's Atmosphere, *Methods Comput. Phys.*, **4**, 1-28, 1965.

Received February 16, 1990; revised May 29, 1990